RESEARCH PAPER

PCCP
www.rsc.org/pccp

Temperature and pressure dependence of ion–molecule association and dissociation reactions: the $N_2^+ + N_2$ (+ M) ⇔ N_4^+ (+ M) reaction†‡

Jürgen Troe*

Institut für Physikalische Chemie der Universität Göttingen, Tammannstrasse 6, D-37077 Göttingen, Germany

Received 26th November 2004, Accepted 10th February 2005
First published as an Advance Article on the web 22nd February 2005

Thermal dissociation and the reverse association reactions of molecular ions can be represented within the same framework as unimolecular reactions of neutral molecules. However, because of different intra- and intermolecular interaction potentials, some differences between ionic and neutral systems should also be expected. Starting from these generalities, the present article analyzes the temperature and pressure dependences of dissociation/association rates of ion–molecule reaction systems. The reaction $N_2^+ + N_2$ (+ M) ⇔ N_4^+ (+ M) is considered in particular and falloff curves for this reaction are constructed over the temperature range 5–600 K. Falloff corrections are applied to earlier experiments which allows for a representation of the rate coefficients in terms of a limiting low-pressure rate coefficient $k_{ass,0}/[N_2]$ cm^6 molecule^{-2} s^{-1} = $6.8 \times 10^{-29}(300\ K/T)^{2.23} - 5.6 \times 10^{-31}(300\ K/T)^{3.12}$, a limiting high-pressure rate coefficient $k_{ass,\infty}$/cm^3 molecule^{-1} s^{-1} = 8.33×10^{-10} $[1 + 0.069(300\ K/T)^{0.33}]$ and a center broadening factor of the falloff curve $F_c = 0.53 \pm 0.05$ nearly independent of the temperature. Other examples such as the reactions $NH_4^+ + NH_3$ ⇔ $N_2H_7^+$, $C_7H_7^+ + CH_3$ ⇔ $C_8H_{10}^+$, and $C_7H_7^+ + C_2H_5$ ⇔ $C_9H_{12}^+$ are illustrated for comparison.

1 Introduction

Radical–radical association and the reverse thermal dissociation reactions of neutral species play an important role, *e.g.* in combustion and in atmospheric chemical kinetics. The temperature and pressure dependences of their rates are well represented within the framework of unimolecular rate theory and they are documented extensively and in compact form in data evaluations such as refs. 1–4. The corresponding information on ion–molecule reactions, in spite of the importance for various applications, is much less complete and waits for more systematic research. In part this is due to experimental limitations, both in the accessible temperature and pressure ranges. The situation, however, is improving *e.g.* by the use of the CRESU technique towards lower temperatures (see *e.g.* refs. 5–7), the SIFT and flowing afterglow techniques towards higher temperatures (see *e.g.* refs. 8–10), and by the use of the turbulent ion flow tube (TIFT, see *e.g.* refs. 9–12) or REMPI-LIF studies in static and flow systems (see *e.g.* refs. 13 and 14) towards higher gas pressures. With these techniques, one can now envisage measurements over broader ranges of conditions such that compact representations of the rate coefficients $k(T,p)$ as a function of temperature T and pressure p will become available as well.

Obviously $k(T,p)$ should be represented in the same way for ionic as for neutral reactions. Separate formats of data representation, analyses, and terminologies within the fields of ionic and neutral reactions, such as they have often been employed in the past, appear undesirable and should be avoided. Falloff curves characterizing the pressure dependence of $k(T,p)$, *e.g.*, should be treated by RRKM theory such as demonstrated for proton-bound dimers of amines by Olmstead, Lev-On, Golden and Brauman,[15] or by the more advanced versions of unimolecular rate theory available today, see below. Specific rate constants $k(E,J)$ for the fragmentation of neutrals and ions should be expressed in the same way such as illustrated in unimolecular reaction monographies (see *e.g.* refs. 16 and 17). Nevertheless, the interesting question remains in which details of the treatment the neutral and ionic systems differ. The intra- and intermolecular interaction potentials, which are relevant for the reaction, often are of different character which may (or may not) lead to characteristic differences in the rate coefficients $k(T,p)$. This is one of the aspects of the present article.

Another issue is the applicability of phase space theory (PST) which has been used in various investigations particularly of ionic systems (see *e.g.* refs. 18–20). It has become clear that specific rate constants $k(E,J)$ and the corresponding high-pressure rate constants $k(T,p \rightarrow \infty)$ of ion–molecule dissociation/association reactions often can not be described by PST, see *e.g.* the recent refs. 12, 21, 22 and earlier work. On the other hand, product translational distributions[17] in the fragmentation of molecular ions often are well represented by PST: this apparent contradiction needs to be explained. A further question is the effectivity of intermolecular energy transfer in ion–molecule dissociation/association reactions.[11,12] The following analysis of a few model systems tries to shed some light on these issues.

We choose the reaction system $N_2 + N_2^+$ (+ M) ⇔ N_4^+ (+ M) as a representative example because ample experimental information on this system is available[13,23–33] and earlier modellings of the rate constant have been published (see *e.g* refs. 13, 32 and 34). We demonstrate how a quick and simple analysis of the experiments can be made which allows for an orientation about the falloff curve of the reaction and the location of the experiments along this curve. Based on the resulting corrections, tentative limiting low- and high-pressure rate coefficients are obtained. The further analysis compares

† Dedicated to Prof. Michael Buback at the occasion of his 60th birthday.
‡ Presented at the Bunsen Discussion on Chemical Processes of Ions, Marburg, 15–17 September 2004.

DOI: 10.1039/b417945p

these experimental values with tentative theoretical modelling results. The combination of the two parts of the analysis on the one hand leads to improved constructions of experimental falloff curves, low- and high-pressure rate coefficients, and compact data representations. On the other hand, the theoretical analysis is used as a diagnostics for uncertain details of the treatment. We are far from having an accurate theory in hands which predicts rates on the basis of theoretical input alone. In this situation, the combination of experiment and theory can lead to an improved understanding. The present analysis of the N_4^+-system well demonstrates the state of the art. For illustration, the results of the N_4^+-system are also compared with data for the $NH_4^+ + NH_3 \Leftrightarrow N_2H_7^+$, $C_7H_7^+ + CH_3 \Leftrightarrow C_8H_{10}^+$, and $C_7H_7^+ + C_2H_5 \Leftrightarrow C_9H_{12}^+$ reactions.

2 Experimental results

The pressure dependence of the reaction

$$N_2^+ + N_2 (+ M) \rightarrow N_4^+ (+ M) \qquad (1)$$

has been investigated only rarely. Mostly the reaction was assumed to be in the termolecular limiting low-pressure range, although some suspicions about deviations from this limit were expressed, *e.g.* in refs. 31 and 34. Only the REMPI-LIF work by Frost and Sharpe[13] more systematically studied the pressure dependence from 1 to 13 Torr in the bath gas M = N_2, and from 10 to 490 Torr in the bath gas He. Fig. 1 shows the results which cover a certain part of the falloff curve with a transition from third to second reaction order. Tentative falloff curves are drawn as full lines such as described below. The temperature dependence has been studied extensively over the broad range 4–530 K, see refs. 23–33. Fig. 2 shows a plot of $\log k_{ass}/[N_2]$ *vs.* $\log T$ where k_{ass} is the pseudo-second order rate coefficient and experiments in the bath gas M = N_2 are included as full symbols. It has only occasionally been questioned whether the data from Fig. 2 really correspond to the third-order limiting low-pressure rate coefficient of reaction (1) and some deviations from the general trend in ref. 34 were tentatively attributed to falloff effects. However, without data such as shown in Fig. 1 and/or at least a simplified modelling such as demonstrated in the following, corrections for falloff were difficult if not impossible to quantify and falloff effects were difficult to distinguish from experimental artefacts. With the help of our construction of falloff curves, selected experiments at $T < 100$ K in Fig. 2 have been falloff-corrected which led to the shown open symbols, see below. The presence of artefacts in some experiments became also particularly clear when data in the bath gases N_2 and He over wider temperature ranges

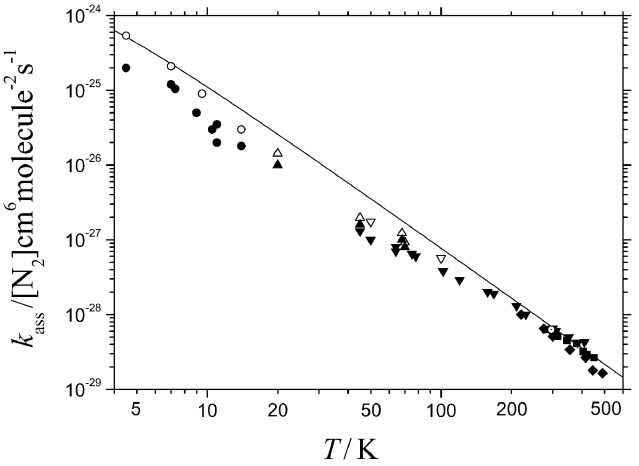

Fig. 2 Temperature dependence of $k_{ass}/[N_2]$ for the reaction $N_2^+ + N_2 (+ N_2) \rightarrow N_4^+ + (N_2)$. Experimental points from ref. 32 (●), ref. 30 (▲), ref. 27 (▼), ref. 31 (■), ref. 33 (◆) and ref. 13 (⊙); modelled curve with eqn. (15) from this work; open symbols = selected falloff-corrected points of $k_{ass,0}/[N_2]$ with correction from this work, see text.

were compared, see Fig. 3. The full lines correspond to our preferred rate coefficients for N_2 (upper curve) and He (lower curve). The pronounced differences between various studies obviously wait for an explanation.

The situation initially appeared even less clear for the reaction

$$NH_4^+ + NH_3 (+ M) \rightarrow N_2H_7^+ (+ M) \qquad (2)$$

for which representations of $\log k_{ass}/[M]$ *vs.* $\log T$ in various bath gases showed quite different and – at first sight – unexplainable slopes while plots of $\log k_{ass}$ *vs.* $\log T$ showed marked deviations from ion–molecule "collision rate coefficients", see Figs. 4 and 5 from ref. 7. A rationalization of experimental results like those shown in Figs. 1–5 can only come from the complete modelling of the temperature and pressure dependences of $k_{ass}(T,[M])$ or $k_{ass}(T,p)$ in the framework of unimolecular rate theory. *E.g.* Fig. 6 shows the results for reaction (2) with M = He from Figs. 4 and 5 in a falloff representation of $\log k_{ass}$ *vs.* log[M] with the parameter T. One realizes that the experimental conditions have corresponded to different locations between the limiting low- and high-pressure ranges. Obviously, one can not provide an analysis of the experimental data before at least a semiquantitative modelling of the falloff curves has been made. Similar to the evaluation of

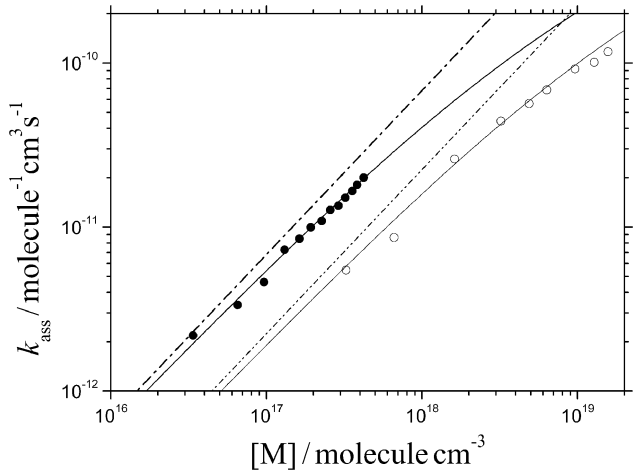

Fig. 1 Pressure dependence at 296 K of the pseudo-second order rate coefficients k_{ass} of the reaction $N_2^+ + N_2 (+ M) \rightarrow N_4^+ (+ M)$ with the bath gases M = He (○) and N_2 (●). Experimental points from ref. 13; modelled falloff curves with eqns. (3), (11) and (14)–(17).

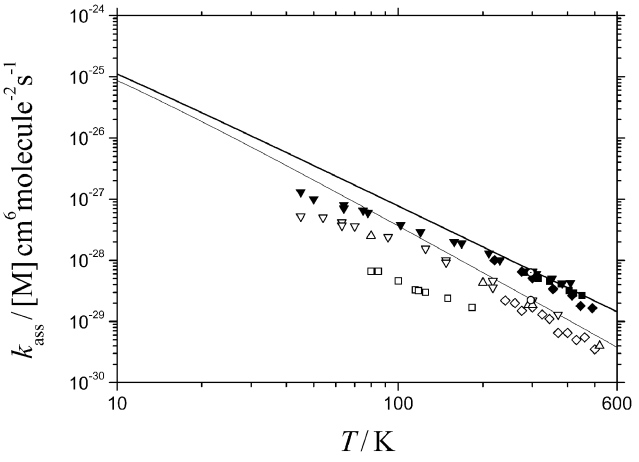

Fig. 3 Temperature dependence of $k_{ass}/[M]$ for the reaction $N_2^+ + N_2 (+ M) \rightarrow N_4^+ (+ M)$. Open experimental points for M = He, filled experimental points for M = N_2, from ref. 13 (⊙ and ○), ref. 33 (◆ and ◇), ref. 31 (■ and □), ref. 27 (▼), ref. 29 (▽), ref. 25 (△). Modelled curves with eqns. (14) and (15) from this work.

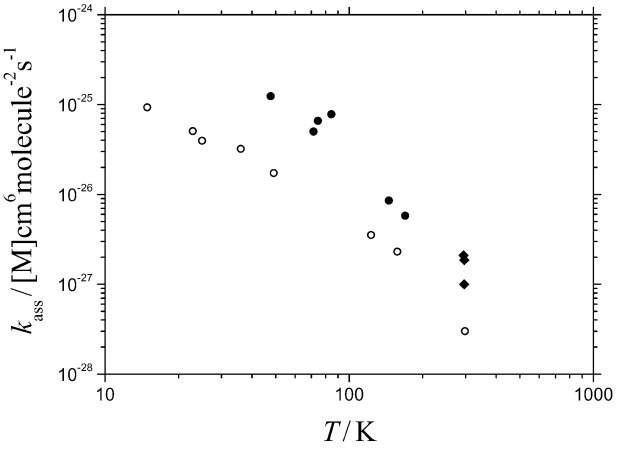

Fig. 4 Temperature dependence of k_{ass}/[M] for the reaction $NH_4^+ + NH_3$ (+ M) → $N_2H_7^+$ (+ M). Experimental points for M = He (O) from ref. 7 and ref. 56 (at 300 K), for M = N_2 (●) from ref. 7 and for M = O_2 and NO (◆) from refs. 57–60.

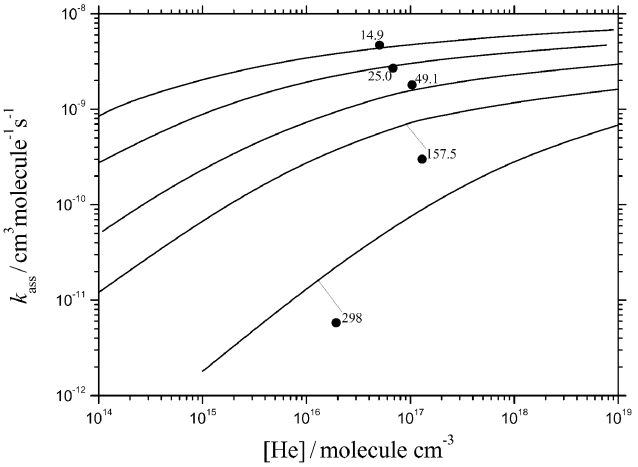

Fig. 6 Falloff representation of data from Figs. 4 and 5 with falloff curves from ref. 7 (numbers in the figure = T/K).

the $N_2H_7^+$-system from ref. 7, we shall illustrate the procedure for the N_4^+-system (1) in the following.

3 Representation of rate coefficients $k(T,p)$

Like for neutral reaction systems, we express the pseudo-first order rate coefficients for dissociation or the pseudo-second order rate coefficients for association in doubly-reduced form

$$\frac{k}{k_\infty} = \left[\frac{k_0/k_\infty}{1 + k_0/k_\infty}\right] F(k_0/k_\infty) \qquad (3)$$

where the limiting low-pressure values k_0 of the rate coefficients k are proportional to the bath-gas concentration [M] and the limiting high-pressure values k_∞ are independent of [M]. The broadening factors $F(k_0/k_\infty)$ use the [M]-proportional ratio k_0/k_∞ as the reduced pressure scale and they characterize the deviation of the actual falloff curve from the Lindemann–Hinshelwood curve (*i.e.* the curve with $F = 1$) by the center broadening factor $F_{cent} = F(k_0/k_\infty = 1)$ and by suitable shape functions.

It is convenient to factorize the low-pressure rate coefficient $k_{diss,0}$ (for dissociation), which in statistical unimolecular rate theory is given by

$$k_{diss,0} = \beta_c Z\,[M] \sum_{J=0}^{\infty} (2J+1) \int_{E_0(J)}^{\infty} f(E,J)\mathrm{d}E, \qquad (4)$$

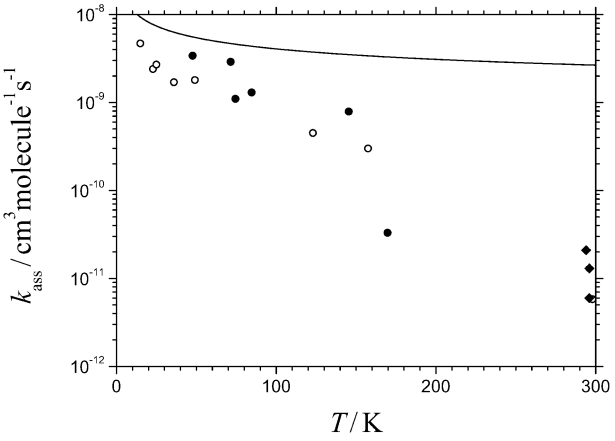

Fig. 5 As Fig. 4, full line: ion-induced + permanent dipole capture rate coefficients, from ref. 7.

with the centrifugal barriers $E_0(J)$ and the equilibrium populations $f(E,J)$, into an expression[35,36]

$$k_{diss,0} = \beta_c Z[M]\{\rho_{vib.h}(E_0)kT/Q_{vib}\}\exp(-E_0/kT)F_E F_{anh} F_{rot} \qquad (5)$$

(for the meaning of the various factors in $k_{diss,0}$, see ref. 36 and the calculations described below). Eqns. (4) and (5) are the results of solving a master equation for intermolecular energy transfer between the bath gas M and the reactant. The properties of this energy transfer, which is rate determining and therefore deserves particular attention, are characterized by the collision efficiency β_c and the collision number Z and they can be related to average step sizes $\langle\Delta E\rangle$ for energy transfer and overall cross sections.[35] It appears inappropriate to call the calculation of the "trivial", statistical thermodynamical, factor $f(E,J)$ a "phase space theory" such as has become common in the ion–molecule community. This practice turns away emphasis from the properties of $\beta_c Z$, *i.e.* from the rate determining process. Instead, the term "phase space theory" should remain reserved to properties of the dissociative process such as specific rate constants $k(E,J)$, k_∞, or product energy distributions; we suggest[37] that it should even be restricted to reactions on isotropic potential energy surfaces only such as this is also the policy of the present approach.

It is also convenient to express the high-pressure rate coefficients for dissociation (k_{diss}) and for association (k_{ass}) in the form[37]

$$k_{diss,\infty} = \sum_{J=0}^{\infty} (2J+1) \int_{E_0(J)}^{\infty} k\,(E,J) f\,(E,J)\mathrm{d}E \qquad (6)$$

or

$$k_{ass,\infty} = f_{el}\left(\frac{kT}{h}\right)\left(\frac{h^2}{2\pi\mu kT}\right)^{3/2} Q_{cent} f_{rigid}(T) \qquad (7)$$

where $f_{rigid}(T) = 1$ in our nomenclature corresponds to "phase space theory" (PST) and f_{el} denotes the fraction of encounters leading into the electronic ground state of the adduct (for the meaning of the various factors in $k_{ass,\infty}$, see ref. 37 and the calculations described below). The centrifugal partition function Q_{cent} is given by

$$Q_{cent} = \sum_{J=0}^{\infty} (2J+1)\exp[-E_0(J)/kT] \qquad (8)$$

where $E_0(J)$ accounts for selected properties of the potential energy surface of the reaction.

k_{diss} and k_{ass} are linked by the equilibrium constant K_c through

$$\frac{k_{ass}}{k_{diss}} = K_c = \left\{\frac{[A]}{[B]\ [C]}\right\}_{eq} = \frac{Q_{vib,rot,el}(A)\exp(E_0/kT)}{Q_{vib,rot,el}(B)\ Q_{vib,rot,el}(C)}\left(\frac{h^2}{2\pi\mu kT}\right)^{3/2} \quad (9)$$

and

$$f_{el} = Q_{el}(A)/[Q_{el}(B)Q_{el}(C)].$$

The shape of the broadening factors $F(k_0/k_\infty)$ will be illustrated below. It should be repeated that, at various levels of simplification, the expressions commonly used in the ion community and notably elaborated by Bates, Herbst, Bowers and others (see *e.g.* refs. 38–43) are equivalent to eqns. (3)–(9) from standard statistical unimolecular rate theory of neutral reactions, and a common language appears more than timely today.

4 Simplified falloff curves and falloff corrections

The detailed theoretical determination of the factors entering eqns. (3)–(9) in general meets with a lot of uncertainties and unknown molecular properties. For this reason an iterative combination of experimental and theoretical information appears necessary. We demonstrate this approach in the following. We start with a very simple estimate of falloff corrections to be applied to the experiments presented in Figs. 1 and 2.

To a first approximation we assume that the experimental data given in Fig. 2 have been obtained near to the low-pressure third-order limit of reaction (1). We then also assume that the high-pressure second-order limiting value of k_{ass} is of the order of the Langevin ion-induced isotropic dipole capture rate constant

$$k_{ass,\infty} \approx k_L = 2\pi\sqrt{\alpha q^2/\mu} \quad (10)$$

With the polarizability $\alpha = 1.77 \times 10^{-24}$ cm^3 of N_2 this leads to $k_{ass,\infty} \approx 8.33 \times 10^{-10}$ cm^3 molecule^{-1} s^{-1}. To a first approximation, the centers of the falloff curves then are located at those values of $[N_2]$ were $k_{ass,0} = k_{ass,\infty}$. With $k_{ass,0}/[N_2]$ from Fig. 2 and $k_{ass,\infty}$ from eqn. (10) one obtains $[N_2]_{cent} \approx 4 \times 10^{15}$, 8×10^{16}, 8×10^{17}, 5×10^{18}, 1.4×10^{19} and 4×10^{19} molecule cm^{-3} at $T = 4$, 20, 70, 200, 300 and 500 K, respectively. Falloff corrections, within this first approximation, then are estimated through the approximate relationship[36]

$$F(x) \approx F_{cent}^{1/[1+(\log x/N)^2]} \quad (11)$$

with $x = k_{ass,0}/k_{ass,\infty}$ and $N \approx 0.75$–$1.27 \log F_{cent}$. While the rigorous calculation of F_{cent} is fairly involved, see below, a quick estimate follows from the modelling of ref. 44 where F_{cent}, for "normal cases", are tabulated as a function of the number of transitional modes of the adduct. For the N_4^+-system with four transitional modes, one has $F_{cent} \approx 0.5$ independent of the temperature. Provided that the values of $[N_2]$ applied in the experiments are given, falloff corrections with eqns. (3) and (11) then immediately can be estimated.

Applying the described procedure to the near-third order experiments of Fig. 2, one obtains a second approximation for the experimental $k_{ass,0}$. Repeating the procedure practically does not further change the values. We have selected representative experimental points (full symbols) from Fig. 2 and indicated the corresponding falloff-corrected results by open symbols in Fig. 2. In several publications unfortunately the experimentally used [M] were not given. However, there were enough data which could be falloff-corrected. The shift of $[N_2]_{cent}$ towards smaller values with decreasing temperature makes low-temperature experiments particularly susceptible to these corrections. The free-jet experiments from ref. 32 between 4 and 20 K, which have employed bath-gas concentrations of N_2 between abut 5×10^{14} and 1.5×10^{15} molecule cm^{-3}, and the CRESU experiments from ref. 30, therefore, have been of particular interest. As shown in Fig. 2, considerable falloff corrections to these experiments are suggested by the described simplified procedure. Nevertheless, these corrections are only tentative at this stage and require a validation by a more thorough theoretical modelling such as presented in the following. The apparent agreement between "phase space calculations" of $k_{ass,0}$ and the measured k_{ass}, which was found in ref. 32, on the basis of the present analysis has to be considered as accidental and misleading.

5 Low-pressure rate coefficients for $N_2^+ + N_2$ (+ M) → N_4^+ (+ M)

In this section we compare the derived low-pressure rate coefficients $k_{ass,0}$ of reaction (1) from Figs. 1 and 2 with calculations based on eqns. (5) and (9). These calculations are not as straight-forward as one would like. Information on the essential collisional energy transfer parameters Z and β_c are scarce. It appears reasonable to identify Z with the N_4^+–M capture rate coefficients.[45–48] These are the Langevin rate coefficient $Z = k_L = 5.56 \times 10^{-10}$ cm^3 molecule^{-1} s^{-1} for N_4^+–He collisions and the ion-induced dipole + quadrupole capture rate coefficient[48] for N_4^+–N_2 collisions $Z = 7.20 \times 10^{-10}$ cm^3 molecule^{-1} s^{-1} [1 + 0.069(300 K/T)$^{0.33}$], see Appendix. Collision efficiencies through $\beta_c/(1 - \beta_c^{1/2}) = -\langle\Delta E\rangle/F_E kT$ are linked to average energies $\langle\Delta E\rangle$ transferred per collision.[35,36] For a start, we tentatively identify $\langle\Delta E\rangle/hc$ with the values −180 and −250 cm^{-1} for M = He and N_2, respectively, such as derived from chemical activation experiments[11,12] with excited $C_8H_{10}^+$ and $C_9H_{10}^+$. These values later on are fine-tuned by comparison with the experiments.

The "more trivial" statistical factors in eqn. (5) (being consistent with those in K_c from eqn. (9)) are calculated with vibrational frequencies, rotational constants, and the bond energy E_0, such as summarized in the Appendix. The centrifugal barriers $E_0(J)$ employed in the calculation[36] of the rotational factors F_{rot} in eqn. (5) (and in the centrifugal partition function Q_{cent} in eqn. (8)) have to be determined from the minimum energy path (MEP) potential and, thus, require information on the potential energy surface of the reaction. The *ab initio* calculations from ref. 49 provide some information on this issue. In the valence range, the graphical representation of the N_4^+ potential from ref. 49, for $(r - r_e) \leq 3.8$ Å, leads to a MEP potential of the linear N_4^+ species of Morse type

$$V(r) = D_e\{1 - \exp[-\beta_e(R - R_e)]\}^2 \quad (12)$$

with the parameters $D_e/hc = 9330$ cm^{-1}, $R_e = 2.00$ Å and $\beta_e = 3.31$ Å^{-1}; R here denotes the N–N distance of the two central N atoms. Outside the valence range, the ion-anisotropic induced dipole + quadrupole potential

$$V(r,\vartheta) = -\frac{q^2\alpha}{2r^4} + \left[\frac{qQ}{r^3} - \frac{q^2\Delta\alpha}{2r^4}\right]\left[\frac{3\cos^2\vartheta - 1}{2}\right] \quad (13)$$

is approached (r = center-of-mass distance between N_2^+ and N_2, $\alpha = 1.77 \times 10^{-24}$ cm^3, $\Delta\alpha = 0.7 \times 10^{-24}$ cm^3, $Q = -1.5 \times 10^{-26}$ esu cm^2 from ref. 50). Unfortunately, the *ab initio* calculations of ref. 49 have not been extended up to the range of R-values where the transition between the valence and electrostatic potential occurs. We have, therefore, calculated $E_0(J)$ for a potential which switches abruptly at the crossing of the MEP potentials of eqns. (12) and (13) (the difference between bond lengths R and c.o.m. distances r has to be taken into account). Fig. 7 shows the MEP potentials for eqns. (12) and (13) together with the positions and heights of the

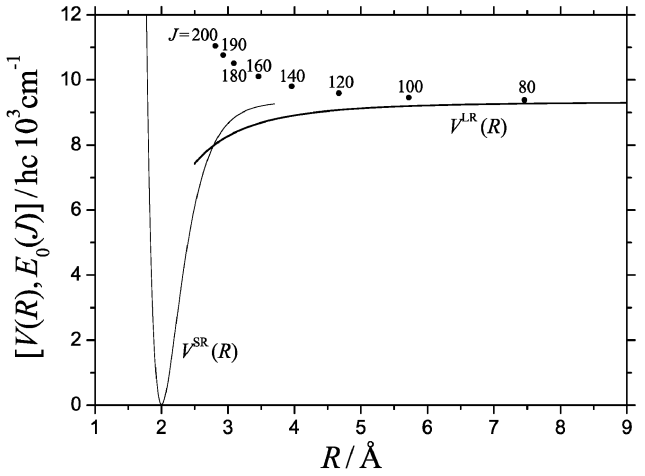

Fig. 7 Minimum energy path potential $V(R)$ and centrifugal energies $E_0(J)$ for the N_4^+-system ($V^{SR}(R)$ = Morse potential from *ab initio* calculations of ref. 49, $V^{LR}(R)$ = ion-anisotropic induced dipole + quadrupole potential, ● = positions and heights $E_o(J)$ of centrifugal barriers, R = length of the central R–R bond in N_4^+).

centrifugal barriers $E_0(J)$. Following the way from $E_0(J)$ to F_{rot} such as described in ref. 36, one obtains F_{rot} such as given in the Appendix. Obviously, with the chosen potential model the long-range potential matters most over a wide temperature range and the valence potential becomes important only at very high T. The same applies to centrifugal partition functions Q_{cent}, see below.

A further point of uncertainty is the anharmonicity correction factor F_{anh}. Using fundamental instead of harmonic frequencies such as done here, a substantial part of the anharmonicity correction is already included but there is additional anharmonicity. Our experience from "normal" triatomic molecules indicates that an additional factor of about $F_{anh} \approx 1.66$ is needed.[51–53] However, this factor is somewhat uncertain and requires more work in the future.

The evaluation of eqns. (5) and (9) is straight-forward. It leads to results which remain most uncertain in the factor $\beta_c Z F_{anh} F_{rot}$. A fine-tuning by comparison with the most reliable experiment, at least at one temperature, can not be avoided. If a calculation of $k_{ass,0}$ would agree with the experiments without fine-tuning, today this still has to be considered as accidental. In our present work we rely most on the results at 296 K from ref. 13 with M = He and N_2 (after minor changes due to the falloff extrapolation, see below) and we fine-tune the $\langle\Delta E\rangle$-values. For M = He, agreement with $k_{ass,0}$(296 K) is found if $\beta_c \approx 0.39$ and $-\langle\Delta E\rangle/hc = 240$ cm^{-1} is chosen (instead of the initial guess of 180 cm^{-1}, see above). The markedly larger value of $k_{ass,0}$(296 K) for M = N_2 would require to increase $-\langle\Delta E\rangle/hc$ from 250 to values above 1000 cm^{-1} where β_c approaches unity and where β_c becomes insensitive to the value of $\langle\Delta E\rangle$. However, it should be emphasized that the fitted β_c- and $\langle\Delta E\rangle$-values also include errors from other factors such as $Z F_{anh} F_{rot}$ such that no safe conclusions on $\langle\Delta E\rangle$ can be drawn for M = N_2. Nevertheless, the unusually large difference between the experimental values of $k_{ass,0}$ in He and N_2, see Fig. 3, points towards unusually efficient energy transfer in N_4^+-N_2 collisions, perhaps due to complex-forming collisions between N_4^+ and N_2. While an apparent ratio $\beta_c(He)/\beta_c(N_2) \approx 0.49$ is derived from the experiments of ref. 13, the apparent ratio $\beta_c(He)/\beta_c(N_2) \approx 0.14$ from ref. 31 in our analysis would lead to an apparent value of $\beta_c(N_2) \approx 2.8$ which would be difficult to understand in terms of uncertainties of other factors. We, therefore, consider the value of the ratio $\beta_c(He)/\beta_c(N_2)$ from ref. 31 as unrealistic and probably due to an unexplained experimental artefact.

Since $\langle\Delta E\rangle$ in the analysis of experiments for neutral systems often has been found to be temperature independent (see *e.g.* ref. 54), we here assume the same and test the predicted temperature dependence of $k_{ass,0}$. Our results over the range 5–600 K can be represented by

$$k_{ass,0}/[He]\ cm^6\ molecule^{-2}\ s^{-1} \approx 2.42 \times 10^{-29} (300\ K/T)^{2.60} - 1.79 \times 10^{-30}(300\ K/T)^{3.15} \quad (14)$$

$$k_{ass,0}/[N_2]\ cm^6\ molecule^{-2}\ s^{-1} \approx 6.80 \times 10^{-29} (300\ K/T)^{2.23} - 5.60 \times 10^{-31}(300\ K/T)^{3.12} \quad (15)$$

where the second terms only matter at low temperatures. The two-term form of Eqns. (14) and (15) was chosen in order to reproduce small deviations of the calculated $k_{ass,0}/[M]$ from simple T^{-n} expressions. Eqns. (14) and (15) are included in Figs. 2 and 3. The agreement with the falloff-corrected experimental values looks very good. However, one should keep in mind that a number of uncertain assumptions have been made such as the values of the anharmonicity correction, $\langle\Delta E\rangle$, the potential leading to F_{rot} and the collision frequency Z being taken as the ion–dipole + quadrupole capture rate constant. In addition, falloff corrections so far came from the simplified method of section 4. The latter procedure requires a more detailed control such as given in the following, but it does not lead to noticeable changes of the derived values of $k_{ass,0}$.

6 High-pressure rate coefficients for $N_2^+ + N_2 \rightarrow N_4^+$

We now consider $k_{ass,\infty}$ for reaction (1). So far only the measurements from ref. 13 have accessed a certain part of the falloff curve, see Fig. 1. However, no reliable extrapolations to the high-pressure limit could be made on the basis of these experiments alone. Instead, $k_{ass,\infty}$ in ref. 13 was fixed by an estimate from AQO theory.[55] Abandoning AQO theory, we now use the more correct SACM/CT treatment from ref. 48, such as described in the Appendix, assuming that the ion-induced dipole + quadrupole potential governs Q_{cent}*. For higher temperatures ($T \rightarrow 600$ K), minor modifications from the valence potential arise which, however, can not be quantified as long as the transition between valence and electrostatic potential in Fig. 7 is not better characterized (see also the analogous investigation of the contribution from valence forces in the $N_2H_7^+$ system described in ref. 7). For this reason, we represent $k_{ass,\infty}$ by the ion-induced dipole + quadrupole potential only. For this potential, the SACM/CT calculations from ref. 48 (for adiabatic dynamics such as realized here) give

$$k_{ass,\infty}/cm^3\ molecule^{-1}\ s^{-1} = 8.33 \times 10^{-10} [1 + 0.069(300\ K/T)^{0.33}] \quad (16)$$

where the first term corresponds to the ion-induced dipole (Langevin) and the second to the ion-quadrupole capture rate constant. Using a value of $k_{ass,\infty}$(296 K) = 8.3×10^{-10} cm^3 molecule^{-1} s^{-1} instead of 9.0×10^{-10} cm^3 molecule^{-1} s^{-1} from eqn. (16), the experimental falloff curve in ref. 13 was also well reproduced employing a broadening factor $F_{cent} \approx 0.5$. However, the question remained whether this estimated value and the employed shape of the modelled falloff curve (similar to the method from section 4), were adequate. This question will be further examined in the following section.

Before moving on to the full falloff curves we come back to the question of the validity of phase pace theory in calculating $k_{ass,\infty}$. In Fig. 8 we compare $k_{ass,\infty}$ from the SACM/CT calculations for the ion-induced dipole + quadrupole potential with the corresponding results for an ion-induced dipole + locked quadrupole potential which is isotropic and hence corresponds to PST. The two rate coefficients are different such that PST does not apply. The difference, *i.e.* the rigidity factor f_{rigid} in eqn. (7), with decreasing temperature approaches the value 0.534 (for the even case $qQ > 0$, see ref. 48). With

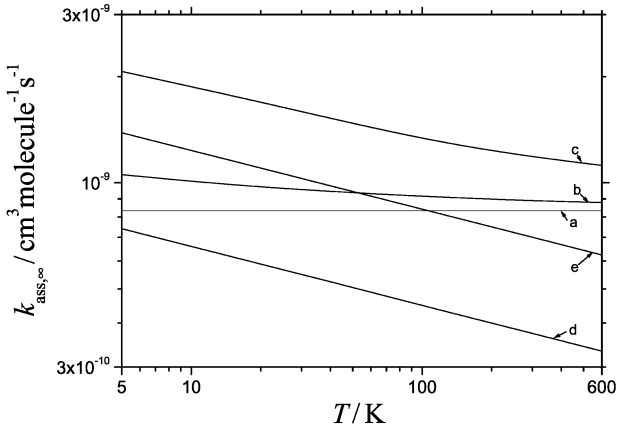

Fig. 8 Limiting high-pressure rate coefficients $k_{ass,\infty}$ for the reaction $N_2^+ + N_2 \rightarrow N_4^+$ (a: Langevin rate coefficient, b: modelling with ion-induced dipole + quadrupole potential, c: as b, but with locked quadrupole = PST, d: modelling with ion-quadrupole potential, e: as d, but with locked quadrupole = PST).

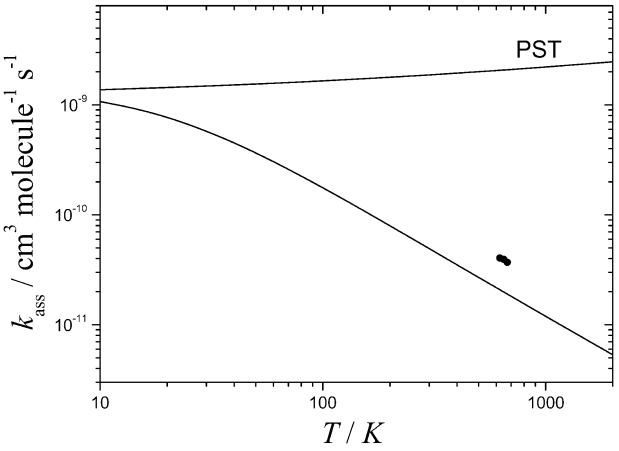

Fig. 9 Limiting high-pressure rate coefficients $k_{ass,\infty}$ for the reaction $C_7H_7^+ + CH_3 \rightarrow C_8H_{10}^+$ (top: PST, lower line: modelling with anisotropic valence/ion-induced dipole potential from ref. 21, ●: experimental points from ref. 22).

increasing temperature, the increasing influence of the isotropic ion-induced dipole short-range potential leads to an increase of f_{rigid}. This may be an artefact of our model since finally the anisotropic valence potential will take over. In any case, however, $k_{ass,\infty}$ is far from the value given by PST. Keeping the rigidity factor for the long-range ion-quadrupole and the short-range valence potential the same, *i.e.* equal to 0.534, the short range-valence/long range-electrostatic switching potential probably leads to an optimum prediction of $k_{ass,\infty}$. This is probably a better estimate of $k_{ass,\infty}$ than given by the ion-induced dipole + quadrupole potential alone. However, in the absence of a better *ab initio* potential in the switching range it appears premature to change $k_{ass,\infty}$. Obviously this uncertainty is of no practical relevance for the range of conditions accessible so far, but it will matter when more high temperature/high-pressure data become available.

Similar remarks apply to the $N_2H_7^+$-system for which the ion-induced dipole + permanent dipole potential was used in the calculations of $k_{ass,\infty}$ from Figs. 5 and 6. Again, due to the anisotropy of the long-range ion-permanent dipole potential $k_{ass,\infty}$ is markedly below the values for the isotropic ion-locked dipole potential used in PST. Also in this case an anisotropic short-range valence potential will cause a further drop of $k_{ass,\infty}$ with increasing T below the values shown in Figs. 5 and 6, see the estimates in ref. 7.

Phase space theory is even more inadequate in cases with weaker isotropic long range potentials and being governed by a markedly anisotropic short range valence potential. We use the $C_7H_7^+ + CH_3 \Leftrightarrow C_8H_{10}^+$ systems and $C_7H_7^+ + C_2H_5 \Leftrightarrow C_9H_{12}^+$ as examples. In these cases thermal dissociation rate coefficients $k_{diss,\infty}$ in the high-pressure limit have been measured[11,12] and related to experimental specific rate constants $k(E,J)$. SACM/CT calculations have been made[21] employing simple switching models between anisotropic short-range valence and isotropic long-range ion-induced dipole components, one parameter of which was calibrated through the experimental $k(E,J)$. One observes that both, the specific and the thermally averaged rate coefficients are far below the PST results, being further away at higher energies and higher temperatures. Figs. 9 and 10 demonstrate the behaviour by a plot of $k_{ass,\infty}$ (converted with K_c from $k_{diss,\infty}$) as a function of temperature. The MEP of the potential causes $k_{ass,\infty}{}^{PST}$ to slightly increase with temperature as compared to the Langevin rate constant. This increase is also an indication of the increasing importance of the valence potential. The rigidity factors f_{rigid} are small, of the order of 10^{-2} to 10^{-3} near 600 K, indicating the dominance of the valence potential under these conditions. Only at very low temperatures the electrostatic range of the potential with $k_{ass,\infty} \Rightarrow k_L$ is predicted to become relevant. In this case the values of the effective Massey parameters = 0.5 and 0.15, for the $C_8H_{10}^+$ and $C_9H_{12}^+$ systems respectively, indicate markedly nonadiabatic dynamics in the transitional modes such that here only SACM/CT and even not conventional variational transition state theory can be used to determine rate coefficients.

The identification of nonadiabatic dynamics may also provide the answer to the apparent paradox mentioned above: rate constants for fragmentation often are far from PST results while product energy distributions often are close to PST predictions. It may well be that the final energy distributions of the dissociation products are being established by nonadiabatic dynamics as well as Coriolis coupling long after the rate-determing dynamical bottlenecks of the reaction have been passed.

7 Reduced falloff curves

Having discussed the detailed estimation of limiting low- and high-pressure rate coefficients $k_{ass,0}$ and $k_{ass,\infty}$, we now proceed to the determination of the falloff curves. Calculating full falloff curves is the most difficult part of the treatment and there is no complete treatment available as yet. However, once $k_{ass,0}$ and $k_{ass,\infty}$ are characterized sufficiently well, doubly reduced falloff curves connecting these rate coefficients are less sensitive to details of the problem. The falloff curves for the

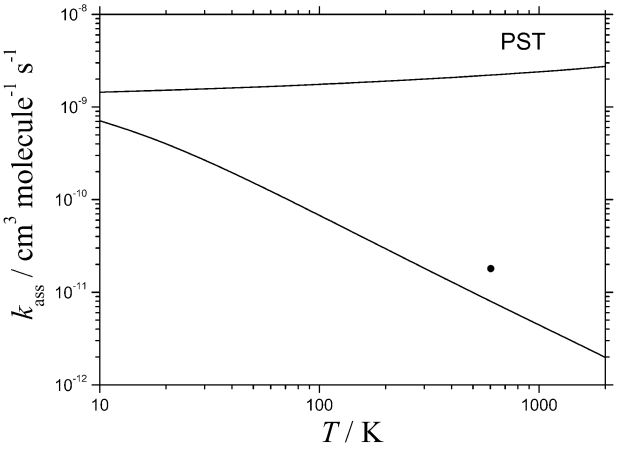

Fig. 10 Limiting high-pressure rate coefficients $k_{ass,\infty}$ for the reaction $C_7H_7^+ + C_2H_5 \rightarrow C_9H_{12}^+$ (top: PST, lower line: modelling with anisotropic valence/ion-induced dipole potential from ref. 21, ●: experimental point from ref. 12).

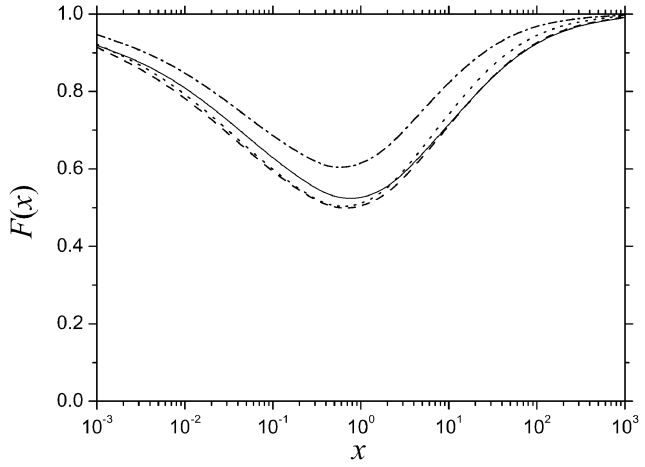

Fig. 11 Broadening factors $F(x)$ for the reaction $N_2^+ + N_2 (+ N_2) \rightarrow N_4^+ + N_2$ ($x = k_{ass,0}/k_{ass,\infty}$; T/K = 5 (—), 50 (--), 300 (···), 600 (---); modelling from this work, see text).

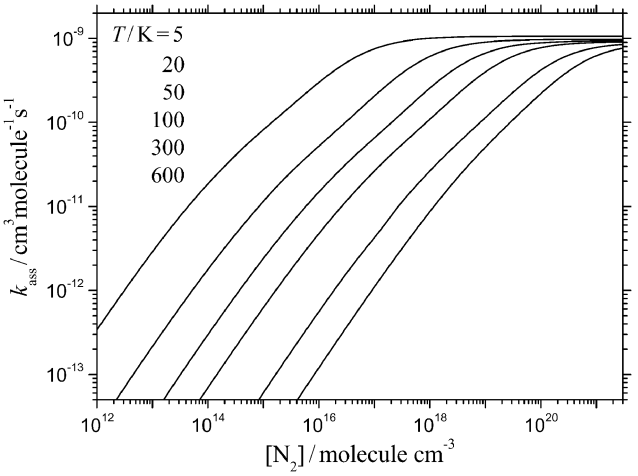

Fig. 13 Modelled rate coefficients $k_{ass}(T, [N_2])$ for the reaction $N_2^+ + N_2 (+ N_2) \rightarrow N_4^+ (+ N_2)$ from this work, see text.

$N_2H_7^+$ system shown in Fig. 5 have been determined in this way.[7] It was shown that PST, accounting for E- and J-dependences of specific rate constants, gives already satisfactory results for the reduced falloff curves, being in contrast to rigid activated complex RRKM theory. The E- and J-dependences of the rigidity factors $f_{rigid}(E,J)$ did not much change the reduced falloff curves from PST. In the following, for the $N_2^+ + N_2 \rightarrow N_4^+$ reaction, we used either the SACM/CT results from ref. 56 or simple PST and we followed the method described in ref. 7.

At first, in Fig. 11 we show the calculated broadening factors $F(k_0/k_\infty)$ of the $N_2^+ + N_2 \rightarrow N_4^+$ reaction as a function of the temperature (including weak collision effects). Second, in Figs. 12 and 13 we provide complete sets of falloff curves for the N_4^+ system which are constructed by means of the calculated broadening factors, eqns. (3), (14) and (16). These curves are completely analogous to Fig. 6 for the $N_2H_7^+$ system. (The curves do not look completely smooth which is not an error of the calculation but a real effect. The shallow dips of the curves are located close to the centers of the falloff curves where $F(k_0/k_\infty)$ has broad minima.) One realizes pronounced shifts of the falloff curves with changing temperatures. At lower temperatures, much lower pressures have to be employed to approach the lower pressure limit of k_{ass} than at higher temperatures. The results well agree with the conclusions from section 4 such that the falloff corrections shown in Fig. 2 essentially remain unchanged. Many investigations, contrary to the assumptions of the authors, have not been performed in the low-pressure

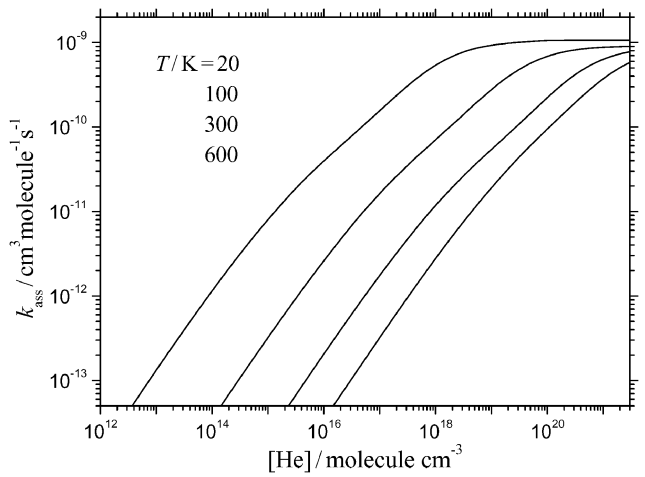

Fig. 12 Modelled rate coefficients $k_{ass}(T, [He])$ for the reaction $N_2^+ + N_2 (+ He) \rightarrow N_4^+ (+ He)$ from this work, see text.

termolecular limit and falloff corrections would have been required before true experimental values of $k_{ass,0}$ could be given. It should be emphasized that this conclusion is quite independent of the remaining uncertainties of the treatment. The construction of falloff curves from ref. 13, which was based on a simpler approach than used here, turned out to nearly coincide with the present more detailed calculations (only a minor difference in the extrapolated $k_{ass,0}$ was observed).

Having done the full falloff calculations, see Figs. 11–13, one may also test the approximate analytical representations of $F(k_0/k_\infty)$ from eqn. (11). A comparison of eqn. (11) with Fig. 11 gives reasonable agreement once F_{cent} is known. Improvements are obtained by replacing eqn. (11) by

$$F(x) \approx F_{cent}^{\{1+[(\log x+0.2)/(N\pm\Delta N)]^2\}^{-1}} \qquad (17)$$

with $F_{cent} \approx 0.53$, $N \approx 1.3$, $\Delta N \approx 0.1$, $+\Delta N$ for $\log x < -0.2$, $-\Delta N$ for $\log x > -0.2$. However, this more complicated expression instead of eqn. (11) appears only necessary when more precise data over wider pressure ranges would be available.

8 Conclusions

We have illustrated the possibilities and uncertainties of today's modelling of the temperature and pressure dependence of rate coefficients $k(T,p)$ for ion–molecule dissociation/association reactions. Our analysis clearly demonstrates the common and different properties of ionic and neutral reaction systems. The reaction $N_2^+ + N_2 (+ M) \rightarrow N_4^+ (+ M)$ has served as a model system for which the determination of $k_{ass,0}$, $k_{ass,\infty}$ and reduced falloff curves were illustrated. A representation with $k_{ass,0}$ from eqns. (14) and (15), $k_{ass,\infty}$ from eqn. (16), and broadening factors of the falloff curve from eqns. (11) or (17), provides a compact format for representing the rate coefficients. This is the same format as routinely employed for neutral radical–radical reactions and it appears advisable that ion–molecule reactions are represented in the same way as neutral radical–radical reactions.

Appendix

Ion-quadrupole capture rate coefficients

Following ref. 48, the effective mass M of the collision system $M = (\mu B/\hbar^2)(Qq/2kT)^{2/3}$ is calculated and found to be much larger than unity such that expressions for adiabatic collisions can be used. These are formulated with the parameters $\theta = \alpha q^{2/3}(2kT)^{1/3}Q^{-4/3}$, $z = 1.352 + \ln\theta$ and $\ln\kappa = 0.2344 + [0.08617z/\sinh z + z^2/16]^{1/2}$. k_{cap} then follows *via* $k_{cap}/k_L = \kappa/(\pi^2\theta)^{1/4}$

and $k_L = 2\pi(\alpha q^2/\mu)^{1/2}$. We use $\alpha = 1.77 \times 10^{-24}$ cm^3 and $Q = -1.5 \times 10^{-26}$ esu cm^2 for N_2.

Molecular parameters[49]

Frequencies of N_4^+: $\nu_i/cm^{-1} = 2275$, 2239, 390, 134 (2) and 91 (2). Rotational constant of N_4^+: $B/cm^{-1} = 0.112$. Bond energy of N_4^+: $E_0/hc = 8908$ cm^{-1}, $D_e/hc = 9330$ cm^{-1}.

Rotational factors $F_{rot}(T)$

F_{rot} in the absence of centrifugal barriers: $F_{rot} = F_{rot\ max} = 467$, 117, 46.7, 23.4, 7.78 and 3.89 for $T = 5$, 20, 50, 100, 300 and 600 K, respectively. F_{rot} for the switching potential from eqns. (12) and (13): $F_{rot} = 52.9$, 21.9, 12.1, 7.72, 3.74 and 2.37. F_{rot} for the long-range potential of eqn. (13): $F_{rot} = 53.8$, 22.4, 12.4, 7.88, 3.81 and 2.4. F_{rot} for the short-range potential of eqn. (12): $F_{rot} = 4.0$, 3.5, 3.1, 2.8, 2.2 and 1.8. All F_{rot} are given for the same series of T as $F_{rot\ max}$.

Acknowledgements

Many helpful discussions with A. A. Viggiano and technical assistance by A. I. Maergoiz are gratefully acknowledged. Thanks are due to M. A. Smith for providing the experimental conditions of ref. 32. Many illuminating discussions with Michael Buback over the past twenty years are also remembered gratefully Financial support of this work by the Deutsche Forschungsgemeinschaft (SFB 357 "Molekulare Mechanismen unimolekularer Reaktionen") and the European Office of Aerospace Research and Development (FA8655-03-1-3034) is acknowledged.

References

1 (*a*) R. Atkinson, D. L. Baulch, R. A. Cox, R. F. Hampson, J. A. Kerr, M. J. Rossi and J. Troe, *J. Phys. Chem. Ref. Data.*, 2000, **29**, 167; (*b*) R. Atkinson, D. L. Baulch, R. A. Cox, J. N. Crowley, R. F. Hampson, R. G. Hynes, M. E. Jenkin, M. J. Rossi and J. Troe, *Atmos. Chem. Phys.*, 2004, **4**, 1461.
2 W. B. Demore, S. P. Sander, R. R. Friedl, D. M. Golden, M. K. Kurylo, R. E. Huie, V. L. Orkin, G. K. Moortgat, A. R. Ravishankara, C. E. Kolb, M. J. Molina and B. J. Finlayson-Pitts, *JPL Publication*, 2003, 02–05.
3 G. P. Smith, D. M. Golden, M. Frenklach, N. W. Moriarty, B. Eiteneer, M. Goldenberg, C. T. Bowman, R. K. Hanson, S. Song, W. C. Gardiner, V. V. Lissianski and Z. Qin, *GRI-Mech 3.0*, 2004, http://me.berkeley.edu/grimech/.
4 (*a*) D. L. Baulch, C. J. Cobos, R. A. Cox, P. Frank, G. Hayman, Th. Just, J. A. Kerr, T. Murrells, M. J. Pilling, J. Troe, R. W. Walker and J. Warnatz, *J. Phys. Chem. Ref. Data.*, 1994, **23**, 847; (*b*) D. L. Baulch, C. T. Bowman, C. J. Cobos, R. A. Cox, Th. Just, J. A. Kerr, M. J. Pilling, D. Stocker, J. Troe, W. Tsang, R. W. Walker and J. Warnatz, *J. Phys. Chem. Ref. Data.*, 2005, **34,** in press.
5 I. W. M. Smith and B. R. Rowe, *Acc. Chem. Res.*, 2000, **33**, 261.
6 B. R. Rowe, J. B. Marquette, G. Dupeyrat and E. E. Ferguson, *Chem. Phys. Lett.*, 1985, **113**, 403.
7 S. Hamon, T. Speck, J. B. A. Mitchell, B. R. Rowe and J. Troe, *J. Chem. Phys.*, 2002, **117**, 2557.
8 S. Williams, A. J. Midey, S. T. Arnold, R. M. Morris, A. A. Viggiano, Y.-H. Chiu, D. J. Levandier, R. A. Dressler and R. R. Berman, *J. Phys. Chem. A*, 2000, **104**, 10336.
9 S. T. Arnold and A. A. Viggiano, *J. Phys. Chem. A*, 2001, **105**, 3527.
10 A. A. Viggiano, T. M. Miller, S. Williams, S. T. Arnold, J. V. Seeley and J. F. Friedman, *J. Phys. Chem. A*, 2002, **106**, 11917.
11 J. Troe, A. A. Viggiano and S. Williams, *J. Phys. Chem. A*, 2004, **108**, 1574.
12 A. I. Fernandez, A. A. Viggiano, T. M. Miller, S. Williams, I. Dotan, J. V. Seeley and J. Troe, *J. Phys. Chem. A*, 2004, **108**, 9652.
13 M. J. Frost and C. R. J. Sharpe, *Phys. Chem. Chem. Phys.*, 2001, **3**, 4536.
14 M. J. Frost, *Phys. Chem. Chem. Phys.*, 2003, **5**, 3169.
15 W. N. Olmstead, M. Lev-On, D. M. Golden and J. I. Brauman, *J. Am. Chem. Soc.*, 1977, **99**, 992.
16 W. Forst, *Theory of Unimolecular Reactions*, Academic Press, New Yorkand London, 1973.
17 T. Baer and W. L. Hase, *Unimolecular Reaction Dynamics. Theory and Experiments*, Oxford University Press, New York and Oxford, 1996.
18 E. E. Nikitin, *Theor. Exp. Chem.*, 1965, **1**, 90.
19 P. Pechukas and J. C. Light, *J. Chem. Phys.*, 1965, **42**, 3281.
20 W. J. Chesnavich and M. T. Bowers, in *Gas Phase Ion Chemistry*, ed. M. T. Bowers, Academic Press, New York and London, 1979, **vol. 1**, p. 119.
21 J. Troe, V. G. Ushakov and A. A. Viggiano, *Z. Chem. Phys.*, 2005, in press.
22 A. I. Fernandez, A. A. Viggiano, A. I. Maergoiz, J. Troe and V. G. Ushakov, *Int. J. Mass Spectrom.*, 2005,in press.
23 M. Meot-Ner and F. H. Field, *J. Chem. Phys.*, 1974, **61**, 3742.
24 R. Johnson, A. Chen and M. A. Biondi, *J. Chem. Phys.*, 1980, **72**, 3085.
25 N. G. Adams and D. Smith, *Chem. Phys. Lett.*, 1981, **79**, 563.
26 T. D. Märk and H. J. Oskam, *Phys. Rev. A*, 1981, **4**, 1445.
27 H. Böhringer and F. Arnold, *J. Chem. Phys.*, 1982, **77**, 5534.
28 J. V. Headley, R. S. Mason and K. R. Jennings, *J. Chem. Soc., Faraday Trans. 1*, 1982, **78**, 933.
29 H. Böhringer, F. Arnold, D. Smith and N. G. Adams, *Int. J. Mass Spectrom. Ion Phys.*, 1983, **52**, 25.
30 B. R. Rowe, G. Dupeyrat, J. B. Marquette and P. Gaucherel, *J. Chem. Phys.*, 1984, **80**, 4915.
31 P. A. M. van Koppen, M. F. Jarrold, M. T. Bowers, L. M. Bass and K. R. Jennings, *J. Chem. Phys.*, 1984, **81**, 288.
32 L. K. Randeniya, X. K. Zeng, R. S. Smith and M. A. Smith, *J. Phys. Chem.*, 1989, **93**, 8031 (typical values of $[N_2]$ in these experiments were between 5×10^{14} and 1.5×10^{15} molecule cm^{-3}).
33 J. A. Guthrie, R. C. Chaney and A. J. Cunningham, *J. Chem. Phys.*, 1991, **95**, 930.
34 R. Patrick and D. M. Golden, *J. Chem. Phys.*, 1985, **82**, 75.
35 J. Troe, *J. Chem. Phys.*, 1977, **66**, 4745; J. Troe, *J. Chem. Phys.*, 1977, **66**, 4758.
36 J. Troe, *J. Phys. Chem.*, 1979, **83**, 114.
37 C. J. Cobos and J. Troe, *J. Chem. Phys.*, 1985, **83**, 1010.
38 E. J. Herbst, *J. Chem. Phys.*, 1980, **72**, 5284.
39 E. J. Herbst, *Chem. Phys.*, 1982, **68**, 323.
40 D. R. Bates, *J. Chem. Phys.*, 1979, **71**, 2318.
41 D. R. Bates, *J. Chem. Phys.*, 1988, **89**, 192.
42 D. R. Bates, *J. Chem. Phys.*, 1989, **90**, 87.
43 L. M. Bass, W. J. Chesnavich and M. T. Bowers, *J. Am. Chem. Soc.*, 1979, **101**, 5493.
44 C. J. Cobos and J. Troe, *Z. Phys. Chem.*, 2003, **217**, 1031.
45 T. Su and W. J. Chesnavich, *J. Chem. Phys.*, 1982, **76**, 5183.
46 J. Troe, *J. Chem. Phys.*, 1987, **87**, 2773.
47 A. I. Maergoiz, E. E. Nikitin, J. Troe and V. G. Ushakov, *J. Chem. Phys.*, 1996, **105**, 6263.
48 A. I. Maergoiz, E. E. Nikitin, J. Troe and V. G. Ushakov, *J. Chem. Phys.*, 1996, **105**, 6270.
49 C. Léonard, P. Rosmus, S. Carter and N. C. Handy, *J. Phys. Chem. A.*, 1999, **103**, 1846.
50 L. F. Phillips, *J. Phys. Chem.*, 1990, **94**, 5265.
51 J. Troe, *Chem. Phys.*, 1995, **190**, 381.
52 R. F. Salzgeber, V. Mandelshtam, Ch. Schlier and H. S. Taylor, *J. Chem. Phys.*, 1988, **109**, 937.
53 M. Mladenović and S. Schmatz, *J. Chem. Phys.*, 1989, **109**, 4456.
54 C. J. Cobos and J. Troe, *Z. Phys. Chem. NF*, 1990, **167**, 129.
55 T. Su and M. T. Bowers, *Int. J. Mass Spectrom. Ion Phys.*, 1975, **25**, 1.
56 A. I. Maergoiz, E. E. Nikitin, J. Troe and V. G. Ushakov, *J. Chem. Phys.*, 2002, **117**, 4201.
57 M. Krishnamurthy, J. A. De Gouw, L. N. Ding, V. M. Bierbaum and S. R. Leone, *J. Chem. Phys.*, 1997, **106**, 530.
58 D. K. Böhme and F. C. Fehsenfeld, *Can. J. Chem.*, 1969, **47**, 2715.
59 L. J. Puckett and M. W. Teague, *J. Chem. Phys.*, 1971, **54**, 4860.
60 F. C. Fehsenfeld and E. E. Ferguson, *J. Chem. Phys.*, 1973, **59**, 6272.